1-1-2014

# Electrospun P2-type Na 2/3 (Fe 1/2 Mn 1/2 )O 2 hierarchical nano fibers as cathode material for sodium-ion batteries

Sujith Kalluri
*University of Wollongong*, sk027@uowmail.edu.au

Kuok Hau Seng
*University of Wollongong*, kseng@uow.edu.au

Wei Kong Pang
*University of Wollongong*, wkpang@uow.edu.au

Zaiping Guo
*University of Wollongong*, zguo@uow.edu.au

Zhixin Chen
*University of Wollongong*

*See next page for additional authors*

# Electrospun P2-type Na 2/3 (Fe 1/2 Mn 1/2 )O 2 hierarchical nano fibers as cathode material for sodium-ion batteries


## Abstract

Sodium-ion batteries can be the best alternative to lithium-ion batteries, because of their similar electrochemistry, nontoxicity, and elemental abundance and the low cost of sodium. They still stand in need of better cathodes in terms of their structural and electrochemical aspects.



## Keywords

type, na, 2, 3, fe, 1, mn, o, electrospun, hierarchical, batteries, cathode, material, sodium, fibers, p2, nano, ion


## Disciplines

Engineering | Science and Technology Studies


## Publication Details

Kalluri, S., Seng, K. Hau., Pang, W., Guo, Z., Liu, H. K. & Dou, S. X. (2014). Electrospun P2-type Na 2/3 (Fe 1/2 Mn 1/2 )O 2 hierarchical nano fibers as cathode material for sodium-ion batteries. ACS Applied Materials and Interfaces, 6 (12), 8953-8958.



## Authors

Sujith Kalluri, Kuok Hau Seng, Wei Kong Pang, Zaiping Guo, Zhixin Chen, Hua-Kun Liu, and S X. Dou

# Electrospun P2-type $Na_{2/3}(Fe_{1/2}Mn_{1/2})O_2$ hierarchical nanofibers as cathode material for sodium-ion batteries

*Sujith Kalluri,[a] Kuok Hau Seng,[a] Wei Kong Pang,[a,c] Zaiping Guo*[*],[a,b] Zhixin Chen,[b] Hua Kun Liu,[a] Shi Xue Dou[a]*

[a]Institute for Superconducting and Electronic Materials, University of Wollongong, NSW 2500, Australia.

[b]School of Mechanical, Materials and Mechatronics Engineering, University of Wollongong, NSW 2500, Australia.

[c]Australian Nuclear Science and Technology Organisation, Locked Bag 2001, Kirrawee DC, NSW 2232, Australia.

ABSTRACT:

Sodium-ion batteries can be the best alternative to lithium-ion batteries, owing to their similar electrochemistry, non-toxicity, elemental-abundance and the low-cost of sodium. They still stand in need of better cathodes in terms of their structural and electrochemical aspects. Accordingly, the present study reports the first example of the preparation of $Na_{2/3}(Fe_{1/2}Mn_{1/2})O_2$ hierarchical

nanofibers by electrospinning. The nanofibers with aggregated nanocrystallites along the fiber direction have been characterized structurally and electrochemically resulting in enhanced cyclability when compared to nanoparticles, with initial discharge capacity of ~195 mAh $g^{-1}$. This is attributed to the well-interconnections among the fibers, with well-guided charge transfers and better electrolyte contacts.

KEYWORDS: batteries, sodium, electrospinning, nanofibers, electrochemistry.

Owing to limited energy resources for the future, it is necessary to look for eco-friendly and affordable renewable energy systems and their systematic utilization by safe and facile energy storage systems.[1-2] Due to superior electrochemistry and cell design, the lithium-ion battery has been predominant in portable applications and also could be in electric vehicles, resulting in depletion of lithium reserves, which is hardly sustainable for future needs.[3] Thus, an alternative that can compete with lithium-ion battery (LIB) technology on the global market is inevitably needed. Sodium is non-toxic, inexpensive, the next lighter and smaller alkali metal other than lithium, has a redox potential suitable for battery applications (0.3 V *vs.* Li), and importantly, is an abundant element, with a similar electrochemistry to that of lithium in LIBs. All these attributes make sodium an alternative to lithium and pave the way for research on feasible sodium-based electrode materials.[4] Surprisingly, the sodium-ion battery (SIB) system is not new; in the 1970s, some researchers conducted early experiments on Na-ion intercalation in certain layered structures,[5,6] although there was little further research due to the commercial dominance of LIBs. Considering the socio-economic and chemical aspects of sodium, there is a need for a new class of sodium-based cathodes and to achieve further understanding of Na-ion

intercalation/deintercalation mechanisms and charge transfers compared with those of the analogous Li materials.

Research on cathode materials for SIBs has been focussed on compounds ranging from polyanions to layered transition-metal oxides, and it is suggested that layered sodium transition-metal oxides show outstanding electrode properties.[7,8] Layered sodium metal oxides are classified as O3- and P2-types, based on the location of the Na-ion at octahedral and prismatic sites, respectively, and there are sub-groups of new phases such as the new O3 and P`3-phases.[9] The P2-type layered oxides such as $Na_{0.6}MnO_2$ and $Na_{0.7}CoO_2$ show improved initial capacity when compared to those of the O3-type $NaMO_2$ (M = Co, Cr, V, $Ni_{0.5}Mn_{0.5}$, etc.), but with poor cyclability.[10-14] To make progress with such cathodes electrochemically and economically, toxic and costly metals such as Cr and Co are need to be replaced with safe and economical Mn and Fe.[8] Various groups have successfully prepared P2-type $Na_x(Mn_{1-y}Fe_y)O_2$ ($x$ = 2/3, $y$ = 1/2) by solid-state reaction, auto-combustion and sol-gel processes,[15-17] and it delivers an excellent initial discharge capacity of ~190 mAh $g^{-1}$ at a low current density in the voltage range of 1.5-4.3 V with optimized proportions of Mn and Fe. Unfortunately, the cyclability of these materials is limited and needs to be improved for large-scale applications. Apart from doping and surface engineering of active materials, nanostructured design of electrodes and electrolyte compositions can contribute to the overall performance of batteries.[18] Nanomaterials have a short Na-ion diffusion distance, relatively less volume expansion during cycling, and better electrolyte contacts due to their high specific surface area, all of which are responsible for improved electrochemical performance in SIBs.[19,20] Nanoparticles have a regular tendency to self-aggregate due to high surface energy, however, resulting in limited contact with the conducting components, which leads to declining net battery performance. Such self-aggregation can be

mitigated by one-dimensional (1D) nanostructures, which could have better contact areas with the electrolyte and offer improved electrochemistry and cycle life.[21,22] Feasible and reliable fabrication techniques are essential for 1D nanostructures. Electrospinning is a low-cost, large-scale, and facile one-pot synthesis technique for continuous nanofibers, and such nanofibrous electrodes offer high porosity, good interfacial contact, and well-guided charge transfer towards the current collector.[23-26]

There have been no reports to date on 1D nanofibrous sodium metal oxide cathodes for SIBs. We have now successfully fabricated electrospun nanofibers of P2-type $Na_{2/3}(Fe_{1/2}Mn_{1/2})O_2$ material and characterized them structurally and electrochemically, demonstrating improved cyclability with better structural stability. We have also attempted to understand the correlation between 1D nanofibers and electrochemical performance.

$Na_{2/3}(Fe_{1/2}Mn_{1/2})O_2$ nanofibers and nanoparticles were prepared by electrospinning and the sol-gel process, respectively and hereafter are designated as NFMO NF and NFMO NP, respectively. Detailed synthesis procedures are explained in the Supporting Information. X-ray diffraction (XRD) patterns for both samples prepared at 900°C are shown in Figure 1. Both patterns appear the same, with well-crystallized sharp reflections associated with the hexagonal phase system and space group P63/mmc, which are well consistent with the literature.[15-17] NFMO is a P2-type structure, with the Na-ions accommodated at two locations in prismatic sites and stacked in between the ordered hybrid octahedral layers of $FeO_6$ and $MnO_6$ [inset of Figure 1].

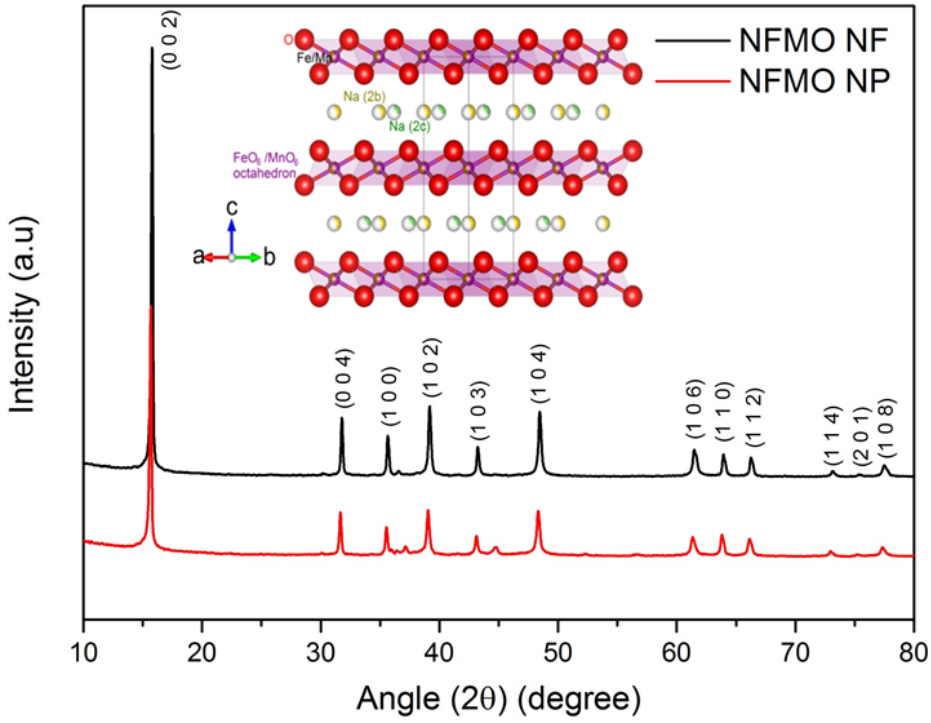


**Figure 1.** XRD patterns of NFMO NF and NFMO NP (inset: crystal structure of P2-type NFMO).

Figure 2(a) shows an scanning electron microscope (SEM) image of the as-spun precursor fibers with average diameter of ~400 nm [see also Figure S1(a) in the Supporting Information]. After calcination, the polyvinylpyrrolidone (PVP) and organic residues are sublimated, resulting in NFMO NF [Figure 2(b)], with average diameter of ~170 nm [Figure S1(b)]. Figure S2 shows an SEM image of NFMO NP with average particle size of ~500 nm. High-resolution transmission electron microscope (HR-TEM) images were obtained to determine the crystallinity and secondary structure of the hierarchical nanofibers. Figure 2(c) is in good agreement with the SEM image in terms of its 1D morphology. Notably, the NFMO nanocrystallites are tightly connected with each other within the nanofiber (as highlighted with contours in Figure 2(c)), and the self-aggregation of nanocrystallites is greatly reduced due to the attachment of nanocrystallites in the nanofiber. Figure 2(d) shows a high-resolution TEM image of the well-

developed nanocrystallite taken at the diffraction condition near the zone axis [$\bar{1}$100]. It shows that the width of the lattice fringes is about 5.4 Å, as marked in Figure 2(d), which is in good agreement with the XRD data and corresponding to the (0 0 2) plane of the hexagonal structure. The longitudinal direction is along [11$\bar{2}$0]. Figure 2(f) presents the energy dispersive X-ray (EDX) spectrum of NFMO NF with the individual elements Na, Fe, Mn, and O.

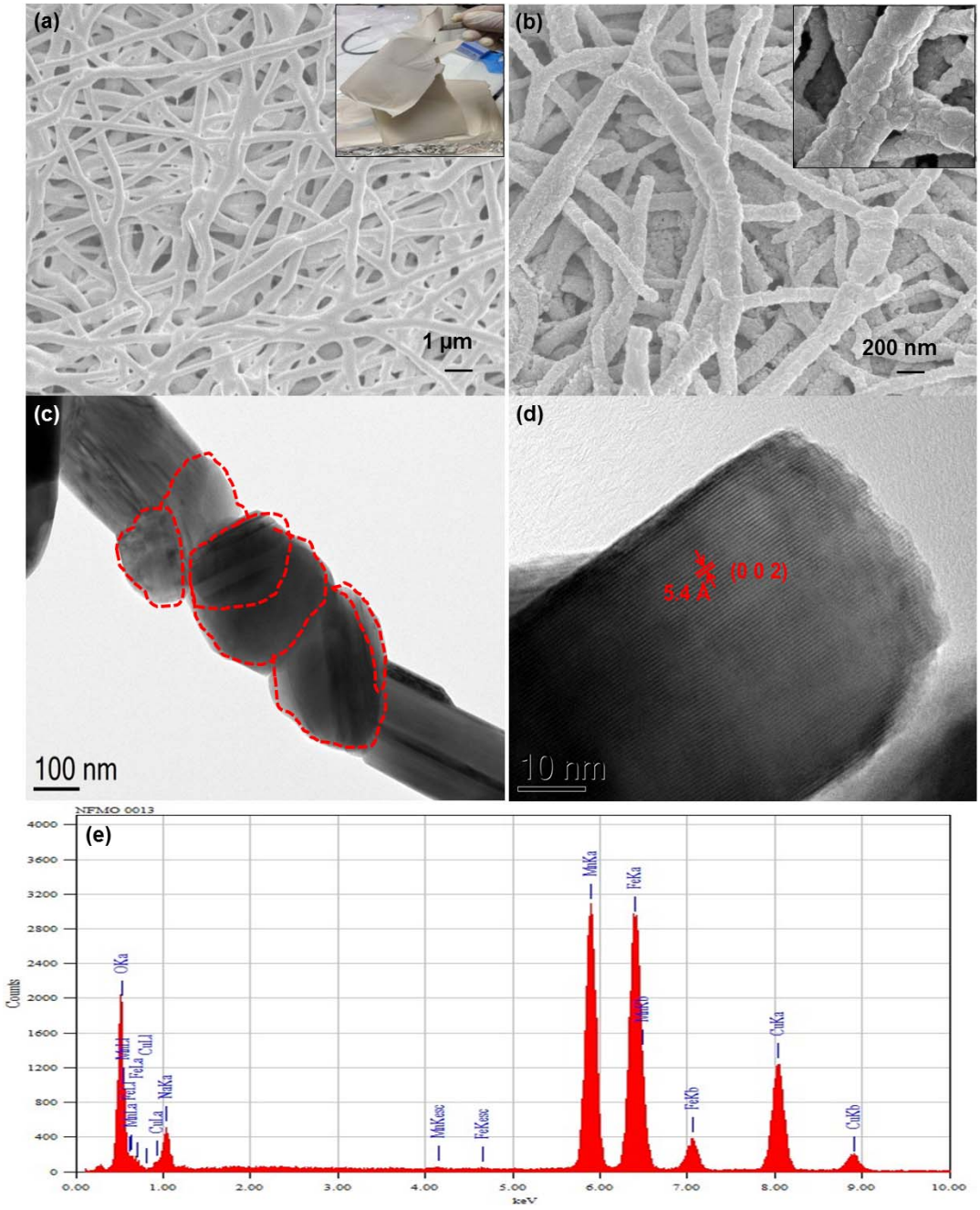

**Figure 2.** SEM images of (a) as-spun nanofibers (inset: photograph of as-spun nanofibrous mat), and (b) NFMO nanofibers (inset: high-resolution image); (c) HR-TEM image of NFMO nanofiber with hierarchical arrangement of nanocrystallites; (d) high-resolution TEM image of a longitudinal nanoparticle taken from near the zone axis $[\bar{1}100]$ showing fringes of (0 0 2) and the longitudinal direction of the particle is $[11\bar{2}0]$; and (e) EDX spectrum.

The electrochemical properties were examined for both samples from charge-discharge curves and cyclic voltammograms (CVs) using a battery analyser and an electrochemical workstation in the voltage range of 1.5-4.2 V. Figure 3(a) shows the charge-discharge behaviour in the initial cycle and the 80$^{th}$ cycle for both samples at 0.1 C current rate (1 C = 260 mA g$^{-1}$). The charge-discharge curves show similar behaviour to that reported elsewhere, with two plateaus at 4 V and 3.4 V, corresponding to phase transitions from P2-type to O2-type with OP4-type as an intermediate phase. The additional plateau around 2.1 V could be attributed to reverse phase transition from OP4-type to P2-type during discharge.[15] Interestingly, NFMO NF showed an improved initial discharge capacity of ~195 mAh g$^{-1}$ when compared to that of NFMO NP (~179 mAh g$^{-1}$). Under the same specifications at the 80$^{th}$ cycle, the discharge capacity is ~167 mAh g$^{-1}$ and ~113 mAh g$^{-1}$ for NFMO NF and NP, respectively, and it is apparent that there is a notable impact of morphology on the stability of NFMO during cycling. Thus, cyclability was evaluated over 80 cycles at the 0.1 C rate, in which the NFMO NF showed an initial capacity decay from ~195 mAh g$^{-1}$ to ~175 mAh g$^{-1}$ for the first few cycles (which could be due to the inherent internal resistance of the cell and the conducting nature of NFMO [27]) and thereafter maintained excellent cyclability [Figure 3(b)], with discharge capacity of ~166 mAh g$^{-1}$ after 80 cycles with 86.4% capacity retention, which is a significant improvement when compared to that of the NP (60.5% capacity retention with the discharge capacity of ~113 mAh g$^{-1}$). The enhanced capacity

and cyclability could be attributed to the well-guided charge transfer kinetics and better wettability of the well-interconnected and highly porous nanofibrous network with respect to the electrolyte over cycling, whereas the NP sample delivered relatively poor capacity retention, which could be attributed to pulverization of the material, less contact of the active material with the electrolyte due to possible self-aggregation of nanoparticles over cycling, and also the relatively larger crystallite size. Such self-aggregation is barely seen for the nanofibers because of the hierarchical crystallite formation at localized sites along the fiber structure during the calcination, which reduces the diffusion in the sintering process.[23] In addition, capacity fade can be observed for the NP sample from the initial cycle to the final cycle, which may be due to the volumetric expansion of the material during repeated Na-ion intercalation/deintercalation processes during cycling and loss of electrical contact between the active material and the current collector.

To understand the impact of morphology on rate performance, both samples were characterized at various rates from 0.1 C to 15 C. The NFMO NF samples featured slightly improved rate performance when compared to NFMO NP. At the high current rates of 1 C, 2 C, and 5C, the NFMO NF sample showed good discharge capacity values when compared to NFMO NP [see Figure 3(c)]. This is attributed to the minimal polarization of the NF electrodes when compared to the NP ones. At the very high rates of 10 C and 15 C, however, for both samples, the discharge capacity values are dramatically diminished to the range of 70 mAh $g^{-1}$ to 33 mAh $g^{-1}$. The charge-discharge curves of both electrodes at various current rates from 0.1C to 15C [see Figure S3(a-b)], reveal that with increasing rate, the two voltage plateaus at 4 V and 3.4 V are gradually diminishing, which could be attributed to the polarization of the electrodes, hindering reversible phase transitions from P2-type to O2-type and leading to corresponding

deterioration in the crystal structure of the active material, thereby decreasing Na-ion intercalation/deintercalation reactions.[8] These reactions are further confirmed by the CVs (Figure 3(d)), with Na as reference and counter electrode in the voltage range of 1.5-4.2 V at the scan rate of 0.1 mV $s^{-1}$. Two pairs of peaks are observed in both the anodic and cathodic sweeps at 2.6 *vs.* 1.9 V and 4.1 *vs.* 3.4 V, corresponding to redox reactions of $Mn^{3+}/Mn^{4+}$ and $Fe^{3+}/Fe^{4+}$, respectively. [28, 29] The phase transition from quasi-reversible P2-type to O2-type due to less Na content upon extraction corresponds to the anodic peak at 4.1 V. This phase change is associated with slight oxygen layer dislocation in the crystal structure of NFMO, resulting in octahedral phase. During reduction, the octahedral phase is converted back to hexagonal phase.[29,8] These voltage plateaus associated with phase transitions are in good agreement with the corresponding charge-discharge curves.

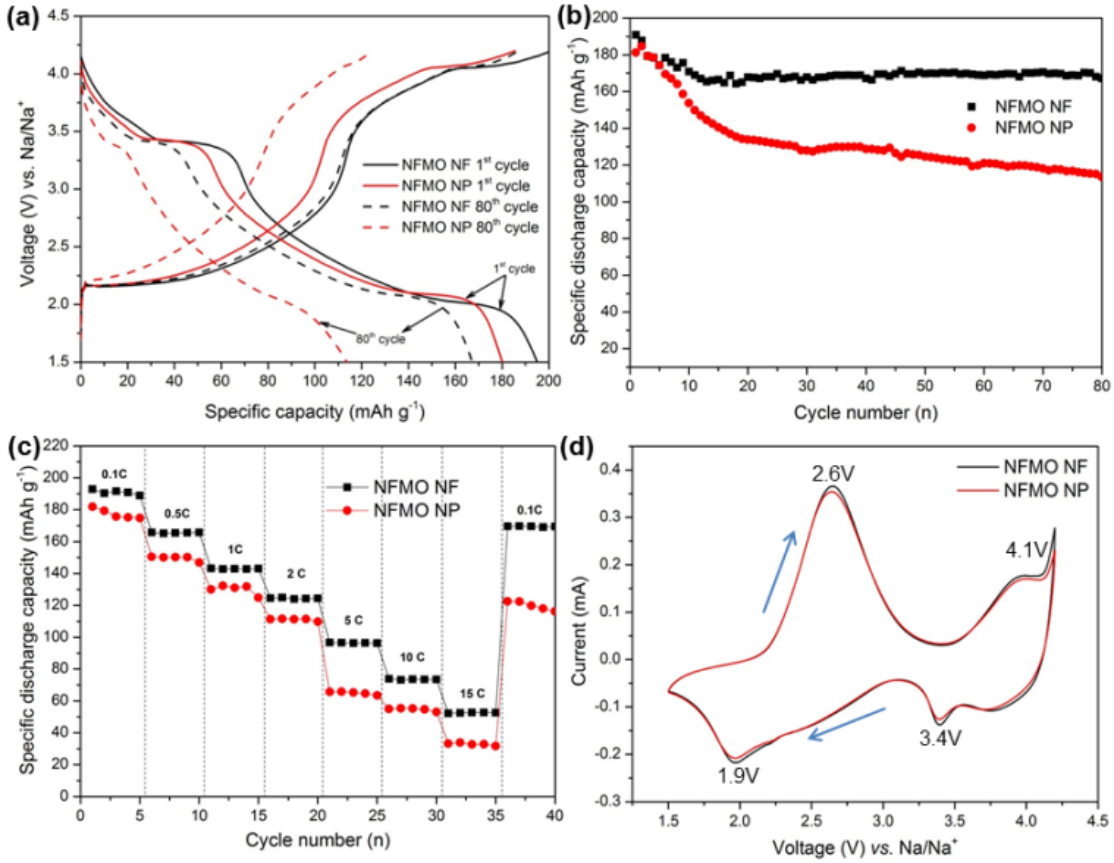

**Figure 3.** (a) Charge-discharge curves of NFMO NF and NP at the initial and 80$^{th}$ cycles at the 0.1 C current rate; (b) corresponding cycling stability; (c) rate performance; and (d) cyclic voltammograms of NFMO NF and NP at the scan rate of 0.1 mV $s^{-1}$. The voltage range is 1.5-4.2V.

Various reasons are proposed for the improved electrochemical performance of the NFMO NF over that of NFMO NP. During the calcination of the as-spun nanofibers, NFMO nanocrystallites are formed at localized sites along the direction of fiber growth [schematic illustration in Figure 4(a)], which is also evident from HR-TEM and SEM analyses [see Figure 3(b-c)]. Such hierarchical growth of nanofibers thereby prevents sintering and self-aggregation,[23,30] whereas nanoparticles without a well-defined morphology have a tendency to self-aggregate, as shown in Figure 4(b). Thus, 1D NFMO nanofibers take advantage of their large effective contact area and consequent better wettability with the electrolyte during cycling, which significantly contributes to improved performance. In addition, the charge transfer kinetics in the active material also influences the electrochemical conductivity. NFMO NFs display well-guided transport behaviour, with long mean free paths of charge carriers (Na-ions and electrons), as shown in Figure 4(a), which improves the electronic and ionic conductivities. The proposed mechanism is evident from the electrochemical impedance spectroscopy (EIS) studies and *ex-situ* SEM analysis, as shown in Figure S4(a-b) and S5(a-b), respectively. EIS measurements were performed to understand the conductivity profiles of the NFs and NPs. The Nyquist plots present the lower charge transfer resistance of 47 Ω for NFMO NF when compared to that of NFMO NP (140 Ω) before cycling, and the same trend is followed even after 80 cycles. *Ex-situ* SEM analysis of both electrodes after 40 cycles revealed the excellent structural stability with well-defined hierarchical structure of the NFs and the self-agglomeration of NPs, as shown in Figure

S5. Further studies relating to the improvement of rate performance at very high current rates and understanding the interfacial properties need to be conducted.

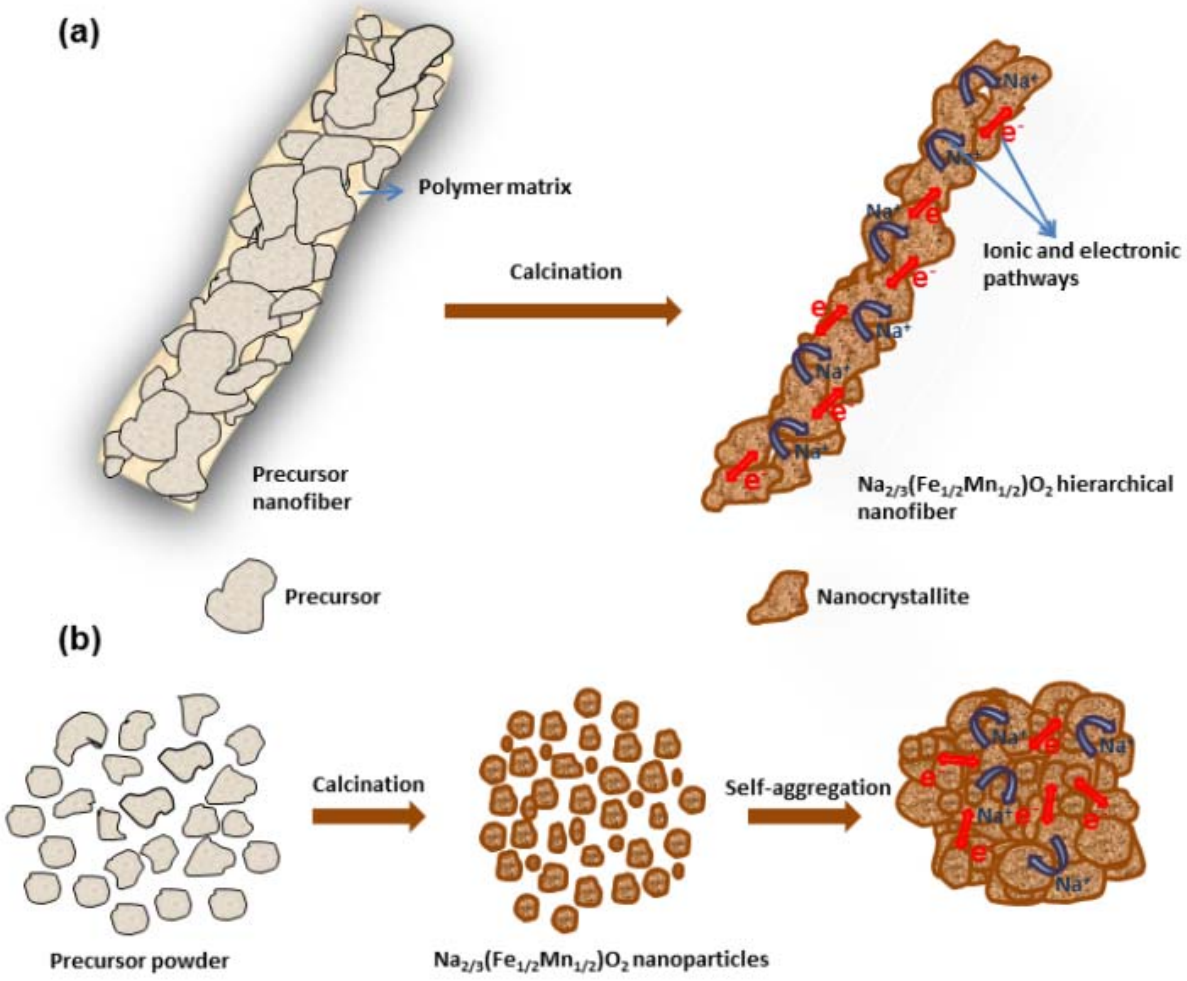


**Figure 4.** Formation mechanism and charge transfer pathways in (a) hierarchical NFMO NF and (b) NFMO NP.

To summarize, structurally stable P2-type $Na_{2/3}(Fe_{1/2}Mn_{1/2})O_2$ hierarchical nanofibers were fabricated by electrospinning. The hierarchical arrangement is formed during the calcination from ordered stacking of nanocrystallites along the direction of fiber growth. These nanofibers showed enhanced electrochemical performance in SIBs, with an initial discharge capacity of

~195 mAh $g^{-1}$ and improved cyclability with capacity retention of 86.4% over 80 cycles. These hierarchical structures are unique in terms of being well-interconnected for charge conductivity and well-guided diffusion pathways. Such hierarchical nanofibers could be one of the potential cathode candidates for SIBs.

## ASSOCIATED CONTENT

The Supporting Information consists of an experimental section with characterization techniques, fiber diameter and particle size distributions of NFMO NF and NP, respectively, with an SEM image of NFMO NP. It also includes the charge-discharge behavior of NFMO NF and NP at various rates, electrochemical impedance plots and ex-situ SEM images of NFMO NF and NP after 20 cycles. This material is available free of charge via the Internet at http://pubs.acs.org."

## AUTHOR INFORMATION

**Corresponding Author**

* Email: zguo@uow.edu.au

## ACKNOWLEDGMENT

Financial support provided by the Commonwealth of Australia and Automotive CRC 2020 is gratefully acknowledged. The authors would like to acknowledge use of facilities at the UOW Electron Microscopy Centre and to thank Dr. Tania Silver for critical reading of the manuscript.

## REFERENCES

(1) Pan, H.; Hu, Y. S.; Chen, L. Room-temperature Stationary Sodium-ion Batteries for Large-scale Electric Energy Storage. *Energy Environ. Sci.* **2013**, *6*, 2338-2360.

(2) Dunn, B.; Kamanth, H.; Tarascon, J. M. Electrical Energy Storage for the Grid: A Battery of Choices. *Science* **2011**, *334*, 928-935.

(3) Tarascon, J. M.; Armand, M. Issues and Challenges Facing Rechargeable Lithium Batteries. *Nature* **2001**, *414*, 359-367.

(4) Slater, M. D.; Kim, D.; Lee, E.; Johnson, C. S. Sodium-Ion Batteries. *Adv. Funct. Mater.* **2013**, *23*, 947-958.

(5) Paranat, J. P.; Olazcuag, R.; Devalett, M.; Fouassie, C.; Hagenmuller, P. Sur quelques Nouvelles Phases de Formule $Na_xMnO_2$ ($x \leqslant 1$). *J. Solid State Chem.* **1971**, *3*, 1-5.

(6) Whittingham, M. S. Chemistry of Intercalation Compounds: Metal Guests in Chalcogenide Hosts. *Prog. Solid State Chem.* **1978**, *12*, 41-99.

(7) Masquelier, C.; Croguennec, L. Polyanionic (Phosphates, Silicates, Sulfates) Frameworks as Electrode Materials for Rechargeable Li (or Na) Batteries. *Chem. Rev.* **2013**, *113*, 6552-6591.

(8) Buchholz, D.; Chagas, L. G.; Winter, M.; Passerini, S. P2-type Layered $Na_{0.45}Ni_{0.22}Co_{0.11}Mn_{0.66}O_2$ as Intercalation Host Material for Lithium and Sodium Batteries. *Electrochim. Acta* **2013**, *110*, 208-213.

(9) Yoncheva, M.; Stoyanova, R.; Zhecheva, E.; Kuzmanova, E.; Vassileva, M. S.; Nihtianova, D.; Carlier, D.; Guignard, M.; Delmas, C. Structure and Reversible Lithium Intercalation in a New P′3-phase: $Na_{2/3}Mn_{1-y}Fe_yO_2$ (y = 0, 1/3, 2/3). *J. Mater. Chem.* **2012**, *22*, 23418-23427.

(10) Komaba, S.; Takei, C.; Nakayama, T.; Ogata, A.; Yabuuchi, N. Electrochemical Intercalation Activity of Layered $NaCrO_2$ *vs* $LiCrO_2$. *Electrochem. Commun.* **2010**, *12*, 355-358.

(11) Komaba, S.; Murata, W.; Ishikawa, T.; Yabuuchi, N.; Ozeki, T.; Nakayama, T.; Ogata, A.; Gotoh, K.; Fujiwara, K. Electrochemical Na Insertion and Solid Electrolyte Interphase for Hard-Carbon Electrodes and Application to Na-Ion Batteries. *Adv. Funct. Mater.* **2011**, *21*, 3859-3867.

(12) Delmas, C.; Braconnier, J. J.; Fouassier, C.; Hagenmuller, P. Electrochemical Intercalation of Sodium in $Na_xCoO_2$ bronzes. *Solid State Ionics.* **1981**, *3-4*, 165-169.

(13) Berthelot, R.; Carlier, D.; Delmas, C. Electrochemical investigation of the P2-$Na_xCoO_2$ phase diagram. *Nat. Mater.* **2011**, *10*, 74-80.

(14) Lu, Z.; Dahn, J. R. In Situ X-Ray Diffraction Study of P 2 - $Na_{2/3}[Ni_{1/3}Mn_{2/3}]O_2$. *J. Electrochem. Soc.* **2001**, *148*, A1225-A1229.

(15) Yabuuchi, N.; Kajiyama, M.; Iwatate, J.; Nishikawa, H.; Hitomi, S.; Okuyama, R.; Usui, R.; Yamada, Y.; Komaba, S. P2-type $Na_x[Fe_{1/2}Mn_{1/2}]O_2$ made from Earth-Abundant Elements for Rechargeable Na Batteries. *Nat. Mater.* **2012**, *11*, 512-517.

(16) Mortemard de Boisse, B.; Carlier, D.; Guignard, M.; Delmas, C. Structural and Electrochemical Characterizations of P2 and New O3-$Na_xMn_{1-y}Fe_yO_2$ Phases Prepared by Auto-Combustion Synthesis for Na-Ion Batteries. J. Electrochem. Soc. **2013**, *160*, A569-A574.

(17) Xu, J.; Chou, S. L.; Wang, J. L.; Liu, H. K.; Dou, S. X. Layered P2-$Na_{0.66}Fe_{0.5}Mn_{0.5}O_2$ Cathode Material for Rechargeable Sodium-Ion Batteries. *ChemElectroChem* **2014**, *1*, 371-374.

(18) Zhou, S.; Wang, D. Unique Lithiation and Delithiation Processes of Nanostructured Metal Silicides. *ACS Nano* **2010**, *4*, 7014-7020.

(19) Chan, C. K.; Peng, H.; Liu, G.; Mcilwrath, K.; Zhang, X. F.; Huggins, R. A.; Cui, Y. High-Performance Lithium Battery Anodes Using Silicon Nanowires. *Nat. Nanotechnol.* **2008**, *3*, 31-35.

(20) Liu, J.; Xia, H.; Xue, D.; Lu, L. Double-Shelled Nanocapsules of $V_2O_5$-Based Composites as High-Performance Anode and Cathode Materials for Li Ion Batteries. J. *Am. Chem. Soc.* **2009**, *131*, 12086-12087.

(21) Brezesinski, T.; Wang, J.; Tolbert, S. H.; Dunn, B. Ordered Mesoporous R-$MoO_3$ with Iso-oriented Nanocrystalline Walls for Thin-Film Pseudocapacitors. *Nat. Mater.* **2010**, *9*, 146-151.

(22) Ge, J.; Zhang, Q.; Zhang, T.; Yin, Y. Core-Satellite Nanocomposite Catalysts Protected by a Porous Silica Shell: Controllable Reactivity, High Stability, and Magnetic Recyclability. *Angew. Chem. Int. Ed.* **2008**, *47*, 8924-8928.

(23) Hagen, R.; Lepcha, A.; Song, X.; Tyrra, W.; Mathur, S. Influence of Electrode Design on the Electrochemical Performance of $Li_3V_2(PO_4)_3$/C Nanocomposite Cathode in Lithium Ion Batteries. *Nano Energy* **2013**, *2*, 304-313.

(24) Thavasi, V.; Singh, G.; Ramakrishna, S. Electrospun Nanofibers in Energy and Environmental Applications. *Energy Environ. Sci.* **2008**, *1*, 205-221.

(25) Kalluri, S.; Seng, K. H.; Guo, Z.; Liu, H. K.; Dou, S. X. Electrospun Lithium Metal Oxide Cathode Materials for Lithium-ion Batteries. *RSC Adv.* **2013**, *3*, 25576-25601.

(26) Denton, A. R.; Ashcroft, N. W. Vegard's Law. *Phys. Rev. A* **1991**, *43*, 3161-3164.

(27) Liu, G.; Xun, S.; Vukmirovic, N.; Song, X.; Velasco, P. O.; Zheng, H.; Battaglia, V. S.; Wang, L.; Yang, W. Polymers with Tailored Electronic Structure for High Capacity Lithium Battery Electrodes. *Adv. Mater.* **2011**, *23*, 4679-4683.

(28) Yuan, D.; Hu, X.; Qian, J.; Pei, F.; Wu, F.; Mao, R.; Ai, X.; Yang, H.; Cao, Y. P2-type $Na_{0.67}Mn_{0.65}Fe_{0.2}Ni_{0.15}O_2$ Cathode Material with High-capacity for Sodium-ion Battery. *Electrochim. Acta* **2014**, *116*, 300-305.

(29) Thorne, J. S.; Dunlap, R. A.; Obrovac, M. N. Structure and Electrochemistry of $Na_xFe_xMn_{1-x}O_2$ ($1.0 \leqslant x \leqslant 0.5$) for Na-Ion Battery Positive Electrodes. *J. Electrochem. Soc.* **2013**, *160*, A361-A367.

(30) Mai, L.; Xu, L.; Han, C.; Xu, X.; Luo, Y.; Zhao, S.; Zhao, Y. Electrospun Ultralong Hierarchical Vanadium Oxide Nanowires with High Performance for Lithium Ion Batteries. *Nano Lett.* **2010**, *10*, 4750-4755.

SYNOPSIS

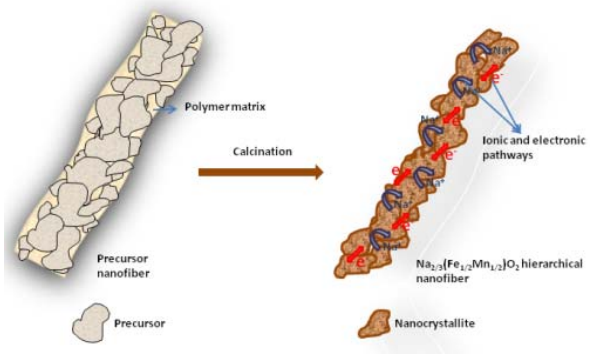
Polymer matrix
Calcination
Precursor nanofiber
Ionic and electronic pathways
$Na_{2/3}(Fe_{1/2}Mn_{1/2})O_2$ hierarchical nanofiber
Precursor
Nanocrystallite

# SUPPORTING INFORMATION

## Electrospun P2-type $Na_{2/3}(Fe_{1/2}Mn_{1/2})O_2$ hierarchical nanofibers as cathode material for sodium-ion batteries

Sujith Kalluri,[a] Kuok Hau Seng,[a] Wei Kong Pang,[a,c] Zaiping Guo,[*a,b] Zhixin Chen, [b] Hua Kun Liu,[a] and Shi Xue Dou[a]

[a]*Institute for Superconducting and Electronic Materials, University of Wollongong, NSW 2500, Australia.*

[b]*School of Mechanical, Materials and Mechatronics Engineering, University of Wollongong, NSW 2500, Australia.*

[c]*Australian Nuclear Science and Technology Organisation, Locked Bag 2001, Kirrawee DC, NSW 2232, Australia.*

[*]*Corresponding Author:* *zguo@uow.edu.au (Prof. Zaiping Guo)*

*Tel: +61-2-4221 5225, Fax: +61-2-4221 5731*

**Experimental:**

### Preparation of $Na_{2/3}(Fe_{1/2}Mn_{1/2})O_2$ nanofibers and nanoparticles

The precursor solution is prepared by dissolving stoichiometric amounts of sodium acetate, iron nitrate, and manganese acetate (all from Sigma-Aldrich with 99% purity) in a mixed solvent of ethanol and N,N-dimethylformamide (DMF). The selection of solvents (ethanol and DMF) is based on their compatibility with the electrospinning process. After stirring for an hour, 10 wt. % polyvinylpyrrolidone (PVP, 1,300,000 g/mol) is added to the resultant solution. After overnight stirring, electrospinning is carried out at room temperature by transferring the precursor solution into a syringe with a 21G stainless steel needle and feeding it into the electrospinning unit (NanoNC, South Korea) at constant parameters: applied voltage: 20 kV, tip to collector distance: 11 cm, feed rate: 0.8 ml $h^{-1}$ and relative humidity (RH): ~25%. After electrospinning, the as-spun nanofibrous mats are collected from the Al foil collector and calcined in a step-wise process as follows: 1° C/min, 350°C, 2h; 2° C/min, 500°C, 2h; and 3° C/min, 900°C, 2 h in compressed-air

atmosphere. Then, the resultant $Na_{2/3}(Fe_{1/2}Mn_{1/2})O_2$ nanofibers (hereafter designated as NFMO NF) are quenched down to room temperature and stored in an Ar-filled glove box. The purpose of the step-wise calcination process in the case of the nanofibers is to protect their structure from collapse during the calcination process by employing slow heating rates in a step-wise fashion.

For the baseline reference sample, the same precursor solution is dried in a drying oven at 100°C overnight and further calcined at 900°C for 2 h in compressed-air atmosphere. The thus obtained $Na_{2/3}(Fe_{1/2}Mn_{1/2})O_2$ nanopowder (hereafter designated as NFMO NP) is quenched down to room temperature.

**Sample characterization**

Structural and crystallographic properties for both NFMO NF and NFMO NP were obtained by X-ray powder diffraction (XRD, GBC MMA) with Cu-Kα radiation. Morphological studies were performed using scanning electron microscopy (SEM, JEOL JSM-7500, Japan) and high-resolution transmission electron microscopy (HR-TEM, JEOL JEM-2010, Japan). Fast Fourier transform (FFT) analysis on the HR-TEM images was performed using digital micrograph software. The fiber diameter and particle size distributions were calculated using ImageJ software. For *ex-situ* SEM characterization after 40 cycles, the coin-cells of NFMO NF and NP were disassembled in a glove box, washed three times with diethyl carbonate (DEC), and dried in the glove box. The thus obtained samples were characterized with SEM, and the corresponding images are shown in Figure S5(a-b).

**Electrochemical characterization**

The electrochemical properties of the as-prepared samples were evaluated in CR2032 coin-cells assembled in an Ar-filled glove box (MBraun, Germany) in the half-cell configuration. Both the

NFMO NF and the NFMO NP cathodes were prepared by milling the active material with carbon black (Super P, TIMCAL, Switzerland) and polyvinylidene fluoride (PVDF) (80:10:10) with N-methyl-2-pyrrolidone (NMP, Sigma-Aldrich) in planetary mixer (Kurabo Mazerustar, Japan). The resultant slurries were coated on Al current collectors by traditional doctor blading and dried in a vacuum oven at 120°C overnight. The coin-cells were assembled using Na disks (Sigma-Aldrich, USA) as counter electrode, porous glass fiber (Milli pore, Australia) as the separator, and 1M $NaClO_4$ in propylene carbonate (PC) as the electrolyte, with 2 wt.% fluoroethylene carbonate (FEC) as an additive. The FEC electrolyte additive acts as a stabilizing agent for the solid electrolyte interphase (SEI) film and helps in improving the Na-ion intercalation/de-intercalation kinetics and thus the cycle life as shown in Figure S7.[1,2] Galvanostatic charge-discharge behaviour was investigated using an automatic battery analyzer (Land, China). A Biologic VMP3 electrochemical workstation was used to collect cyclic voltammograms (CVs) and Nyquist plots. The CV curves were collected with the scan rate of 1 mV $s^{-1}$ and Na-foil as the counter electrode, while the impedance Nyquist plots were collected in the frequency range of 100 kHz to 100 mHz at open circuit voltage. Since this NFMO material is highly sensitive to moisture/air, all the post-synthesis characterizations of both samples were conducted under highly controlled inert conditions. In order to understand the stability of this material in air/moisture, XRD patterns were collected for three successive weeks after exposing the material to air/moisture, as shown in Figure S6. This reveals the structural degradation with time and possibly the formation of some by-products due to the high reactivity of Na with air/moisture.

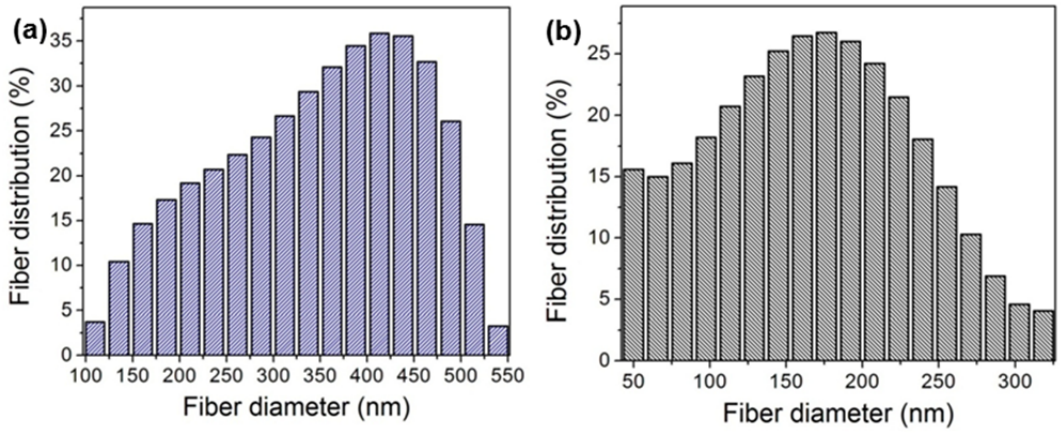


**Fig. S1:** Fiber diameter size distribution of NFMO NF (a) as-spun and (b) heat-treated.

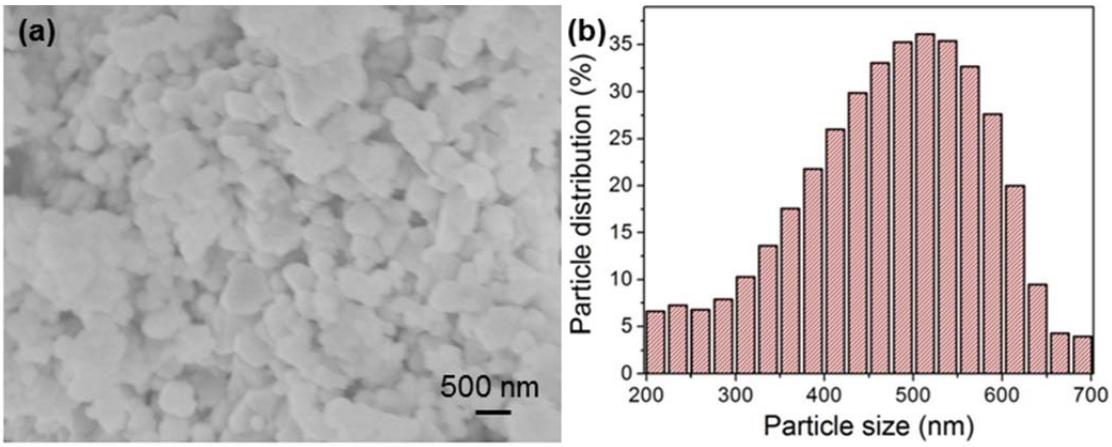


**Fig. S2:** (a) SEM image of NFMO NP and (b) particle size distribution

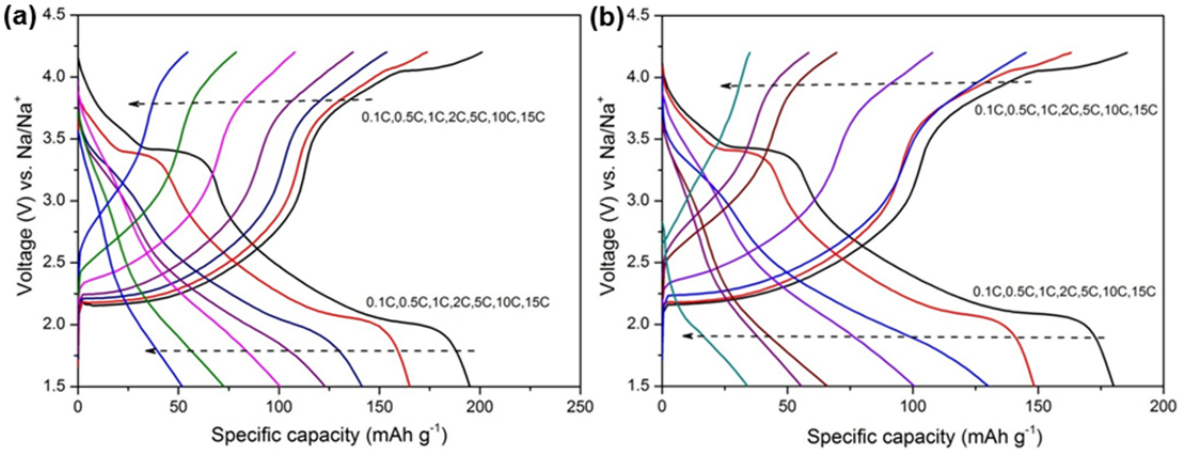

**Fig. S3:** Charge-discharge curves at various current rates measured in the voltage range of 1.5 - 4.2 V for (a) NFMO NF and (b) NFMO NP.

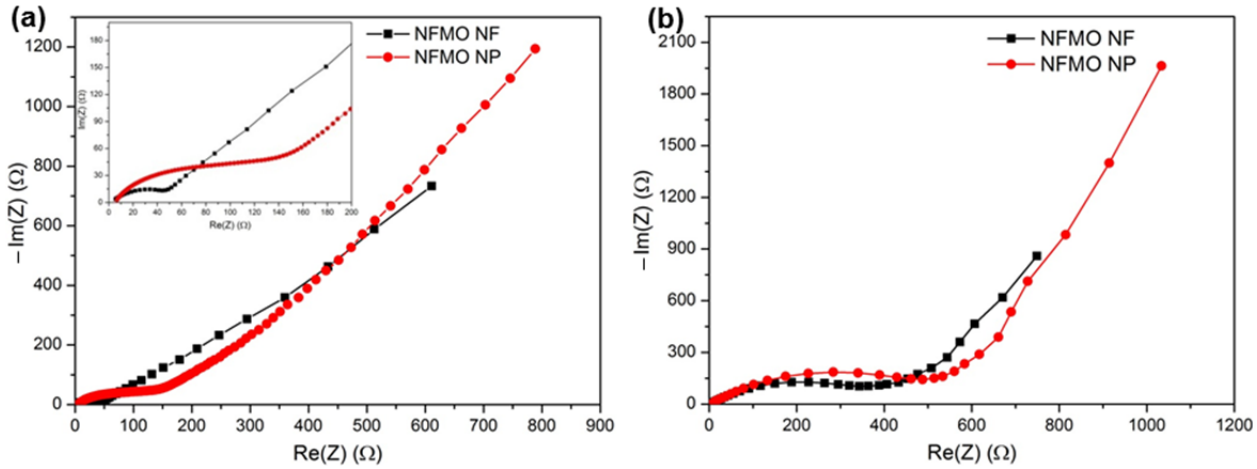


**Fig. S4:** Electrochemical impedance spectroscopy Nyquist plots of NFMO NF and NFMO NP (a) before cycling (inset: highly magnified region of plot) and (b) after cycling, with all plots collected at open circuit voltage (OCV) in the frequency range of 100 kHz to 100 mHz.

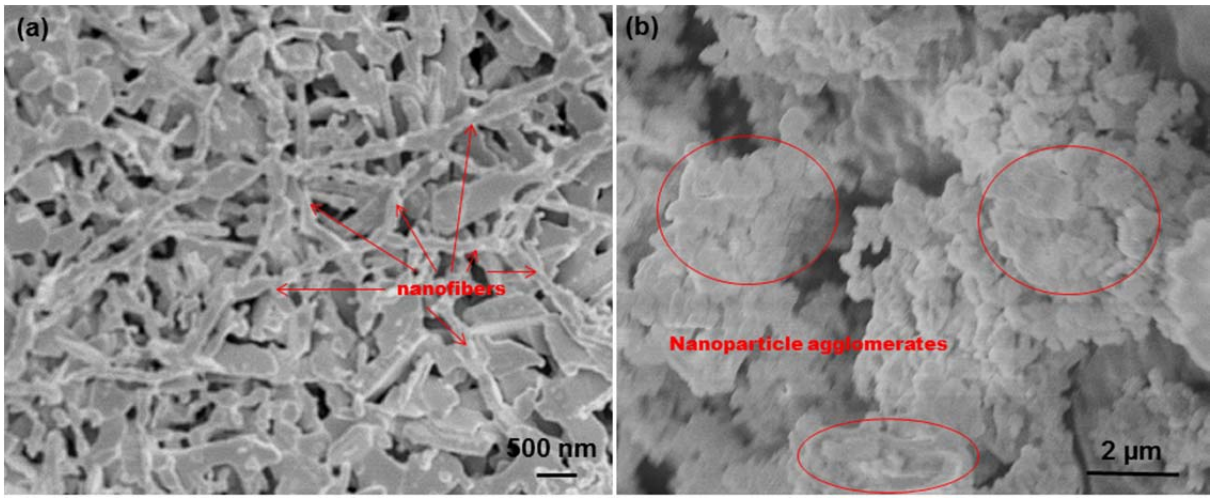


**Fig. S5:** *Ex-situ* SEM images of (a) NFMO NF and (b) NFMO NP after electrochemical cycling.

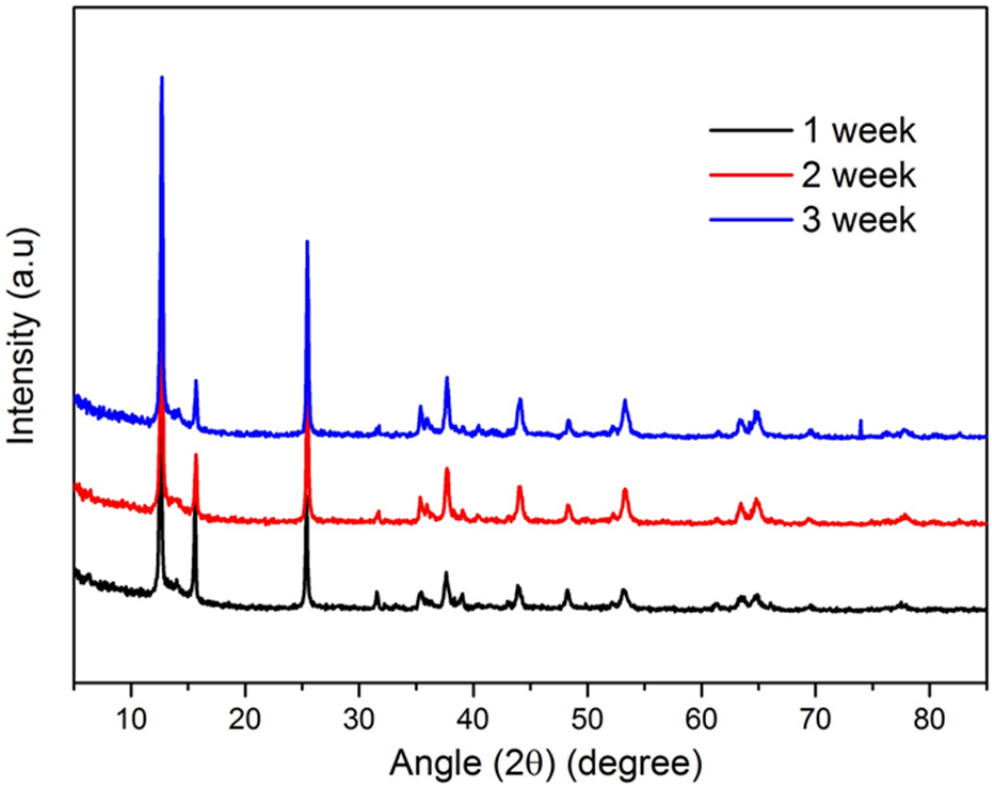


**Fig. S6:** XRD patterns of NFMO after exposure to moisture /air for three successive weeks.

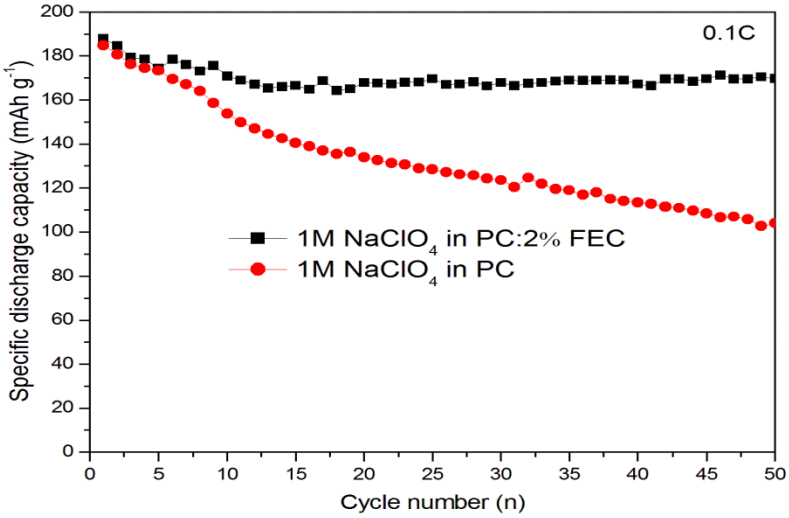


**Fig. S7:** Cycling stability of NFMO NF with and without FEC electrolyte additive at 0.1 C rate.

REFERENCES

(1) Darwiche, A.; Marino, C; Sougrati, M. T.; Fraisse, B.; Stievano, L.; Monconduit, L. Better Cycling Performances of Bulk Sb in Na-Ion Batteries Compared to Li-Ion Systems: An Unexpected Electrochemical Mechanism. *J. Am. Chem. Soc.* **2012**, *134*, 20805-20811.
(2) Etacheri, V.; Haik, O.; Goffer, Y.; Roberts, G. A.; Stefan, L. C.; Fasching, R.; Aurbach, D. Effect of Fluoroethylene Carbonate (FEC) on the Performance and Surface Chemistry of Si-Nanowire Li-Ion Battery Anodes. *Langmuir* **2012**, *28*, 965-976.